Chapter 3

Carrier scattering in diluted nitride and magnetic semiconductors

3.1 Introduction

As discussed in the previous chapter, electron scattering by phonons play a key role in the physics of semiconductor. Furthermore, it was noticed that in order to understand the transport mechanism of carriers with certain probable perturbation in initial momentum and energy through the electrical devices, the interaction of carriers with phonons is essential. In addition to this it is observed that the study of electron – phonon scattering under the dimensional confinement is important and has been considerable interest recently. It is seen that the doping of small amount of N in the gallium arsenide results in the reduction of band gap energy which is useful for many optoelectronic devises. Similarly, the electron transport in DMS is also important to understand the various applications like data storage and memory devices. The present chapter contains the study of theoretical description developed for the carrier-phonon interaction in two dimensional nanostructures and later applied to the dilute nitrides as well as dilutes magnetic semiconductor heterostructures.

3.1.1 Dilute Nitride Semiconductor

There exists nowadays a large interest in the study of large-gap semiconductors-like the III-Nitrides, because of their use in devices, like diodes and lasers, emitting in the blue and near-ultraviolet region [1]. The on-going development of dilute nitrides such as GaNAs and GaInNAs is the focus of a considerable research activity due to their potential application across a range of device applications including lasers [2-7], photo detectors [8], solar cells [9] and transistors [10]. The term dilute nitride is widely used to describe III-V semiconductors consisting of a low nitrogen (<5%) content. It was proposed by Kondow et al [2] that increasing the indium fraction in the quaternary

GaInNAs alloy reduces the band gap but increases the lattice parameter. This makes it possible to balance the nitrogen and indium contents of GaInNAs to target a narrow-band gap material and near lattice parameter matching to substrate materials such as gallium arsenide. The large lattice parameter difference between GaAs and cubic GaN (20%) makes the ternary GaAsN alloy scientifically interesting. Since GaAsN is generally grown on GaAs substrates, strain arising from the mismatch will have an enormous effect on any alloy epilayer properties. Although the fraction of the group V element which is substituted by nitrogen is relatively low, the smaller ionic radius of the nitrogen is observed to dramatically decrease the band gap energy [11, 12] and decrease the lattice parameter with significant increase in electron effective mass and a decrease in electron mobility[13,14]. Furthermore, a new optical transition (E+) above the fundamental band gap energy has been observed [15, 16]. The incorporation of only one percent of nitrogen into GaAs induces a strikingly large reduction of 0.18 eV in the fundamental band gap energy [17]. This reduction is much larger than the changes observed when alloying different III-V compound semiconductors at its percent level. It is now generally accepted that the unexpectedly strong effect of nitrogen on the band gap is related to the fact that replacement of atoms such as As with the much smaller and more electronegative N atom leads to a large, local perturbation of the crystal lattice potential. Extensive experimental and theoretical studies over the past decade have led to several proposals aimed at understanding of the origin of the large band-gap in these systems [18-22]. The effect of nitrogen on the electronic band structure of dilute nitrides can be described in terms of an anti-crossing interaction between localized nitrogen states and the extended conduction-band states of the semiconductor matrix [23]. The interaction leads to a significant modification of the band structure of the dilute III-N-V alloys. Neugebauer and Van de Walle [24] have estimated that the equilibrium solubility of nitrogen in GaAs is of the order of only 2 at. %, making it necessary to use non-equilibrium growth methods. Due to its large miscibility gap GaAsN tends to phase separate when the nitrogen content becomes appreciable [25]; however, nitrogen incorporation up to nearly 15% has been reported using a nitrogen plasma source combined with a relatively low growth temperature of 500 °C on a GaP substrate [26]. The large data available for the quaternary GaInNAs alloy regarding the luminescence from low-nitrogen-containing (<1%) quantum-well-based structures indicates their emission wavelength falls just below 1.3 μm at room temperature for indium contents below 30% [27]. It has also been noted that the addition of higher nitrogen concentrations rapidly degrades the microstructure, preventing its use in optical devices. Some reports of higher nitrogen-containing materials have been made and, in particular, GaInNAs quantum dots with 4% nitrogen have been observed to give peak emission characteristics up to 1.5 μm [28].

3.1.1.1 Bandstructure

(A) Phenomenology

The existence of discrete energy levels due to N impurities in GaP has been known since the 60s. For example, Thomas and Hopfield [29, 30] observed sharp lines in absorption and fluorescence spectra that they attributed to excitons bound to deep-level isoelectronic traps. The most prominent of these was associated with an isolated nitrogen atom substituting for a phosphorus atom with an energy level about 0.02 eV less than the band gap energy. The deeper lines were associated with nitrogen (N-N) pairs. The first observation of such discrete states in GaAs did not come until much later. Wolford *et* al

[31] reported the recombination of an exciton bound to a single nitrogen atom in 1982, whilst Liu *et* al [32, 33] made the first observations of N-N pairs in GaAs in 1990. However, in GaAs, the single nitrogen level appears as a resonant level above the conduction band edge. An interesting property of these energy levels is that they remain pinned with varying nitrogen concentration, implying that the impurities do not interact and confirming their trap-like nature.

As the nitrogen concentration is increased in GaNAs (or GaInNAs), the band-gap exhibits a very large red shift [34,35], characterized by an optical bowing coefficient that appears to be composition dependent and an order of magnitude larger than that in conventional III-V alloys [36]. At the same time, a dramatic increase in the electron effective mass m^* is observed at low N concentrations [37-41], despite the reduction in bandgap, after which m^* varies non-monotonically with x [42]. Additionally, as more nitrogen is incorporated, the pressure [43, 44] and temperature dependence [45] of the band gap is reduced.

(B) Early Theoretical Work

The deep-level trap states due to nitrogen in GaAsP alloys had been predicted by Hjalmarson *et* al [46] in 1980 using a tight-binding model. Although lattice relaxation around the impurity and the effects of second-nearest neighbor atoms were not considered, the results compared well to experimentally observed levels. Here, the adjective 'deep' refers more to the nature of the trap than the binding energy, since in pure GaP the trap is found close to the conduction band edge and resonant with the conduction band in pure GaAs. Early work modeling the effect of dilute concentrations of nitrogen in GaNAs involved first principles density functional theory (DFT), typically using the local density approximation (LDA) to deal with exchange and correlation. Rubio and Cohen [47] predicted a red-shift of the energy gap, due to localization of charge density on the nitrogen sub-lattice. This was explained in terms of large lattice mismatch between As and N and the relative increase in volume seen by the N atom in comparison to GaN. However, no relaxation of the lattice was employed and the calculations were based on ordered alloys. Geometrical relaxation was included by Neugebauer and Van de Walle [48], who found strong optical bowing in zinc-blende superlattices. The calculations predicted a closing of the energy gap, although this can be attributed to the well-known fact that LDA calculations underestimate the bandgap. This problem was addressed by Wei and Zunger [49], who considered the bandgap differences between the alloy and the binaries, hence partially canceling the LDA error. The problem of disorder was addressed by using 'special quasi-random structure' (SQS) supercells, which are designed so as to model the random arrangement of atoms in larger structures. These authors found that in the dilute limit, the conduction bandedge (CBE) wavefunctions are localized, impurity-like states. In this regime, the optical bowing coefficient was found to be large and composition dependent. Moreover, this impurity like region persists at large alloying compositions due to the localized nature of the CBE wavefunctions and consequent lack of overlap between them. To analyze the physical cause of the bandgap bowing, Wei and Zunger identified three contributory components to the bowing coefficient, due to: (i) volume deformation (ii) charge exchange and (iii) structural relaxation. The first of these was found to be relatively small. Charge exchange is due to the atomic orbital energy difference between N and As (related to the greater electronegativity of N). The structural relaxation is due to the size discrepancy between N and As. Subsequent theoretical work can be broadly divided into two complementary approaches. On the one hand, Zunger and co-workers have performed rigorous calculations using the empirical psuedopotential method (EPM). These workers argue that the red-shift and increased effective mass of the CBE is due to mixing of the Γ, L and X bands through the nitrogen impurity potential. On the other hand, the phenomenological band anticrossing (BAC) model proposed by Shan *et al* [43] suggests that the conduction band is split due to the hybridization of the localized nitrogen state and the extended conduction band states of the host semiconductor. This approach has been corroborated and expanded upon by O'Reilly and co-workers using detailed tight-binding (TB) calculations and a derived model based on linear combinations of isolated nitrogen states (LCINS). Whilst both of these approaches accurately describe such phenomenology as the bandgap bowing, pressure dependence of the bandgap and enhanced effective mass, they differ in interpretation. Since the BAC model is the simplest approach and provides a useful common terminology for the description of the band-structure, we shall review this first.

(C) The Band Anticrossing Model

According to the BAC model, the Hamiltonian of the dilute nitride system is given by

$$H = \begin{bmatrix} E_M(x) & V_N(x)^{1/2} \\ V_N(x)^{1/2} & E_N(x) \end{bmatrix} \qquad (3.1)$$

where E_M and E_N are the energies of the matrix semiconductor and localized nitrogen state respectively. Here we have anticipated the x dependence of the matrix interaction element $\langle \psi_M | H | \psi_N \rangle = V_N x^{1/2}$ where $|\psi_M\rangle$ and $|\psi_N\rangle$ are the matrix semiconductor and isolated nitrogen states respectively. This form was not given in Shan *et al*'s original paper, although it has been independently derived by Lindsay and O'Reilly[50] via TB calculations and Wu *et al*[51] using a Green's function approach based on the coherent potential approximation (CPA). O'Reilly et al [52] also derived this form for a Ga_mNAs_{m-1} supercell using a Green's function approach due to Vogl [53]. As we shall see, TB calculations show that E_M and E_N will also have an x dependence, which for the time being we just imply in (3.1).

The energies of the upper and lower bands in the perturbed system, denoted by E_+ and E_- respectively, are found from the resulting eigenvalue equation. The solutions are

$$E_\pm = \frac{1}{2}\left(E_N + E_M \pm \left\{\left[E_N - E_M\right]^2 + 4V_N^2 x\right\}\right) \tag{3.2}$$

From this expression, we can see that E- is red-shifted with increasing nitrogen content. This successfully predicts the observed bowing of the conduction band as well as the pressure [43, 44] and temperature [45] dependence of the energy gap. By assuming a given **k** dependence for E_M (usually parabolic), the effective mass can be calculated, giving good agreement with experiment for very low nitrogen concentrations. Evidence for the existence of the E_+ band was given by Shan *et al*, who identified a E_+ transition in photo modulated reflectance (PR) spectra [43]. Before giving a qualitative explanation of these effects, it is useful to define the fractional Γ character of the bandedge wavefunctions (we assume here that we are dealing with nitrogen in GaAs or GaInAs, which are direct band semiconductors, so that the unperturbed conduction band of interest is indeed the Γ valley - this is not the case in GaP).

In the BAC model, the resultant wave function of the perturbed system will be a linear superposition of the matrix semiconductor and nitrogen wavefunctions:

$$|\psi_{\pm}\rangle = \alpha_M^{\pm}\,\psi_M\rangle + \left(1-\left|\alpha_M^{\pm}\right|^2\right)^{1/2}|\psi_N\rangle \tag{3.3}$$

In this case, the fractional. Γ character is $\left|\alpha_M^{\pm}\right|^2$, i.e., the projection of the matrix wavefunction on $|\psi_{\pm}\rangle$. Now it can be shown that

$$\left|\alpha_M^{\pm}\right|^2 = \left(\frac{(\Delta E)^2(1\pm\theta)/2}{V_N^2 x}+2\right)^{1/2} \tag{3.4}$$

where,

$$\Theta = \operatorname{sgn}(\Delta E)\left(1+\frac{4V_N^2 x}{(\Delta E)^2}\right)^{1/2} \tag{3.5}$$

and. $\Delta E = E_N - E_M$. From this we find that if *EN* > *EM*, in the lower *E*-band $0.5 \le \left|\alpha_M^{+}\right|^2 \le 1$, whilst in the upper $E+$ band $0 \le \left|\alpha_M^{+}\right|^2 \le 0.5$. This implies that E_- is always more extended in nature, whilst E_+ is more localized- often being referred to as a resonant state in the literature. As we shall see, this result is at variance with both EPM and TB calculations.

The reduced pressure dependency can be explained in terms of the pressure insensitivity of the localized nitrogen states. Hence, as the hydrostatic pressure is increased, the matrix semiconductor band edge will be pushed up towards the resonant nitrogen level. As this level drops into the band gap, there will be a transformation from the lowest conduction band states from extended to highly localized, leading to a saturation of the pressure dependence.

At low temperatures, the conduction band edge will be close to the nitrogen energy level. Hence, it will have a reduced Γ character (i.e. be more localized in nature). As such, it will have reduced temperature sensitivity and the initial change in band gap with increasing temperature will be slow. At higher temperatures, more of the higher lying band states will have crossed over the nitrogen level and the band-edge will now have a much greater character (more extended in nature). There should therefore be a transition to more band-like temperature dependence. This is indeed the dependence observed by Uesugi *et al* [45].

(D) The Empirical Psuedopotential Method

An immediate criticism of the BAC model is that it only considers the effect of a single nitrogen impurity. The effect of other localized states due to nitrogen clusters is completely neglected. Moreover, since the matrix interaction element in the BAC model represents the average interaction of the localized states, it cannot account for disorder effects. These issues must be addressed by more detailed calculations.

In the EPM approach employed by Zunger and co-workers [59-63] many different environments can be investigated by constructing large supercells with the substitution N atoms placed on anion sites either at random or according to some rule. Typically, these researchers use SQS supercells mentioned earlier. Structural relaxation is obtained by using the valence force field method (VFF) [64, 65]. Atomic psuedopotential are then constructed and the supercell Hamiltonian is diagonalised to obtain the band energies and wavefunctions.

At very low N concentrations (the *impurity limit*), a resonant impurity state is found above the valley CBE, associated with an isolated nitrogen atom. This state is found to be highly localized with half of the electronic charge within the nearest neighbors cell. However, according to the EPM calculations, this energy level increases rapidly with nitrogen incorporation, becoming too far away from the host CBE to interact with it and produce the bandgap bowing as described in the BAC model. Instead, it is argued that the nitrogen potential causes the mixing of states from many different bands, giving rise to perturbed host states (PHS). It is the behavior of the PHS in the presence of an isolated N state that gives rise to the bandgap bowing. As in the earlier LDA calculations discussed above, the main physical causes of the large bowing were found to be charge exchange and structural relaxation.

The increase in effective mass is attributed to mixing of and *L* states, the effective mass being much greater in the *L* valley than in the valley. As the pressure increases, the -*L* interaction becomes less significant and E- gains greater *X* character. This leads to a repulsion from the *X* state and an even greater effective mass. This mixing of states in *E*- represents a delocalization in momentum space, which implies localization in real space. Recall that in the BAC model, it was shown that the character of *E*- was always greater than 0.5, implying delocalization in real space. The EPM calculations offer no direct evidence of the *E*+ level. Instead, the *E*+ transition is interpreted in terms of a configurational weighted average of the N and *L* levels. An important prediction of the EPM approach is the formation of cluster states (CS) in the bandgap as observed experimentally. These states have little overlap and so do tend to interact or broaden in energy as the nitrogen content increases. The CS are not held responsible for any effect on the optical bowing, since this is found to be large when only isolated N states are present. Thus the bowing is attributed solely to the effect of the latter on the PHS.

As the N content increases, the PHS are found to broaden, moving down into the bandgap and sweeping through the CS. This coexistence of localized states and the PHS is identified as the *amalgamation limit*, characterized by alloy fluctuations. At higher N concentrations, the PHS move past the CS into the *alloy limit*, in which the bandedge states become delocalized and conventional alloy behavior is predicted.

In summary, the EPM method predicts much the same phenomenology as the BAC model, although the interpretation is quite different. Of course, as it stands, the BAC model is an extremely simple one and we would not expect it to compete with detailed calculations in regards to predictions. In the next section, we will find that both the general form and interpretation of the BAC model is supported by supercells calculations using a tight-binding method to find the band-structure. In the meantime, we note that it is agreed that a localized impurity state is formed on the nitrogen site. This is akin to a deep level state, which cannot be represented by a superposition of eigenstates from a single band. Thus, the N state itself can be thought of as a mixture of different band states. It is not entirely clear from the literature whether the mixing of the , L and X valley wavefunctions in the EPM calculations is quantitatively different from mixing with N states, formed from different band states, or whether this is a matter of interpretation.

The issue of the localization/delocalization of *E*- remains an issue, although, as we shall see, this can be reconciled once the BAC model is generalized to deal with the cluster states. The main contention between the EPM calculations and the BAC interpretation seems to be the assertion that the N state moves too far up in energy to interact with CBE.

(E) Tight-Binding and the LCINS Model

Support for the picture of a localized nitrogen state interacting with the host semiconductor conduction band has been offered by O'Reilly and co-workers employing detailed tight-binding calculations [50, 52, 61-63]. As in the EPM method, supercells are constructed and relaxed using VFF calculations, whilst the lattice constant is set according to Vegard's law. The electronic structure is then calculated using an sp^3s^* tight-binding Hamiltonian (i.e. a model in which the sp^3 basis is augmented with the inclusion of an excited *s*-state, s^* on each atom).

For an isolated nitrogen impurity, the existence of a highly localized state resonant within the conduction band was confirmed [50]. Then, by allowing E_M and E_N to vary linearly with x and the BAC matrix element to have the dependence $V_N\, x^{1/2}$, the BAC model could be fitted to the TB calculations for the variation of the bandedge E_{-}. The shift in E_M can be expressed by a linear relation in x

$$E_M(x) = E_M(0) - \alpha_C x \tag{3.6}$$

The fractional character of the CBE also exhibited a good match with the BAC model (the fractional character of the valence band edge was found to vary as $1 - x$). From this, it could be shown using a **k.p** formulation that, despite the decrease in bandgap, the effective mass increases with x. These features demonstrated the agreement between the models for the E- band at least. For the E+ band, however, it was found that no unique *s* like state could be defined. Instead the energy level broadens with increasing N content.

An important consequence for modeling the GaInNAs alloy is the effect of the nitrogen nearest-neighbour environment on the nitrogen state energy and interaction element V_N. O'Reilly *et al* [62] find a near linear increase in the impurity energy as the number of In nearest-neighbors increases. At the same time, V_N decreases so that the overall effect of In incorporation is to weaken the interaction with the host conduction bandedge states.

Since the calculated wavefunction for a single nitrogen impurity is so localized, it was argued that a similar wavefunction could be associated with each N atom in the supercell. It was then shown that the resonant wavefunction implied in the BAC model and calculated for an ordered array of nitrogen atoms could be very well approximated by using a linear combination of isolated nitrogen states (LCINS) associated with the individual N sites. It was found that this approximation remained good up to alloy concentrations of around $x = 0.25$, at which point the overlap between N states could no longer be neglected.

For a random alloy, the approach required adjustment to deal with the inevitable formation of N clusters around shared Ga nearest neighbours. Thus, in addition to a basis set of isolated N states, pairs of N-N states are also introduced (with odd and even parity about the shared Ga site) along with the host semiconductor CBE state. The Hamiltonian for the system can then be found by taking the inner product of the basis states $|\psi_i\rangle$ with the full tight binding Hamiltonian *HTB*

$$H_{ij} = \langle \psi_i | H_{TB} | \psi_j \rangle \qquad (3.7)$$

If the eigenstates of this system are written $|\psi\rangle = \sum_i \alpha_i |\psi_i\rangle$ then these and the eigenvalues E_k can be found by solving

$$\sum_j H_{ij} \alpha_j^k = E_k \sum_j \langle \psi_i | \psi_j \rangle \alpha_j^k \qquad 3.8)$$

Note that the overlap element $\langle\psi_i|\psi_j\rangle$has been included since the basis states are not assumed to be orthogonal to one other. The results are found to be in good agreement with the full TB calculations lending weight to the idea that the perturbation of the CBE is due to the interaction with localized nitrogen states. At low N concentrations, the primary interaction is associated with states near the isolated nitrogen energy level. As the N concentration increases, the energy spectrum of these states broadens and the CBE passes through and hybridises with the N-N clusters, reducing the fractional . character (to less than 0.5 in some cases, in contrast to the BAC model), greatly affecting the effective mass at the band-edge. A remarkable feature of the LCINS model is its ability to predict the observed non-monotonic variation of the effective mass with N concentration14 mentioned earlier.

Instead of calculating the Hamiltonian in (3.7) with the host semiconductor bandedge state $|\psi_M\rangle$included in the basis, an alternative strategy is to first diagonalise the Hamiltonian for the nitrogen states alone and then construct a matrix incorporating the interaction of these states with $|\psi_M\rangle$ [63]. The interaction matrix element is defined by

$$\langle\psi_i|H|\psi_M\rangle = V_i/\sqrt{N_C} \qquad (3.9)$$

where the root of N_C, the number of primitive cells in the supercell, is included due to the normalisation of the basis states and V_i is a material constant. This allows the LCINS model to be rendered in a generalized form of the BAC model, where we now have n bands corresponding to $n-1$ localized nitrogen states.

3.1.2 Dilute Magnetic Semiconductors

Diluted Magnetic Semiconductors (DMSs) are alloys between a non-magnetic semiconductor (e. g. GaAs) and a magnetic element, usually manganese (Mn) [64]. Therefore, semiconducting and ferromagnetic properties coexist in these materials. This leads to important technological applications since the charge and the spin of the electron could be used in the same device. At the same time, the underlying solid state system has an enormous interest for basic science. Dilute magnetic semiconductors are formed by doping the semiconductor matrix with a dilute amount of $3d$ transition metal atoms (magnetic ions). This special class of semiconductors is hoped to form the basis of relatively new class of electronics called spin transfer electronics, or spintronics. In spintronics, the ability to efficiently inject spin-polarized carriers and detect electron spin-orientation forms the basis of this newly emerging class of electronics. The inclusion of Mn into the host, introduces a $3d$ energy level in the energy gap. This energy level is considered an acceptor level since it is closer to the valence band energy. These localized $3d$ energy states of the magnetic ion are coupled to one another through carrier mediation.

Several theoretical models have predicted that the addition of Mn to GaN produces a spin-polarized impurity band within GaN's band gap, and that carrier mediated ferromagnetism in GaMnN occurs when the Fermi level (E_F) is located within this impurity band [65-67]. Therefore the location of E_F will determine the occupancy of this impurity band and thus the availability of carriers to mediate ferromagnetism.

The possibility of controlling both the charge and the spin of the electron has attracted the interest of researchers for several decades. Magnetic semiconductors, such as Europium chalcogenides and semiconducting spinels that have a periodic array of magnetic atoms were extensively studied in the late 1960s.

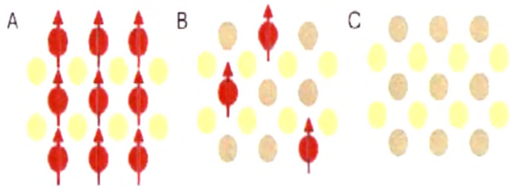

Fig. 3.1 Three types of semiconductors: (a) a magnetic semiconductor, which has a periodic array of a magnetic element, (b) a diluted magnetic semiconductor (DMS), an alloy between a nonmagnetic semiconductor and a magnetic element and (c) a non-magnetic semiconductor, which contains no magnetic ions [64].

However, the crystal structure of such magnetic semiconductors is completely different from that of the most commonly used semiconductors (e. g. Si and GaAs) and the crystal growth of those materials is notoriously difficult. On the other hand, diluted magnetic semiconductors (Fig. 3.1) are based on widely known semiconductors like GaAs that can be doped with impurities to change their properties, usually to p- or n- type. III-V DMSs are defined in an analogous way and are the most important DMSs studied mainly due to their high Curie temperature (T_C), the highest of all DMSs. In fact, the interest in this field was boosted by the demonstration in 1996 that ferromagnetic transition temperatures in excess of 100 K can be achieved in manganese doped gallium arsenide, (Ga, Mn)As [68], much higher than the previous record of only 7.5 K for (In, Mn)As [69]. Recent advances in $Ga_{1-x}Mn_xAs$ have demonstrated that electrical control of their spin properties can be used for the manipulation and detection of magnetic signals. The Mn^{2+} ions in these alloys provide magnetic moments, and at the same time act as a source of valence-band holes that mediate the Mn^{2+}-Mn^{2+} interactions. This coupling results in the ferromagnetic phase.

Among the problems in the production of DMS samples is the low solubility of magnetic elements in III-V semiconductors. Since the magnetic effects are often proportional to the concentration of magnetic ions, x, it is necessary to introduce a sizable amount of magnetic moments (a few percent or more) for the material to develop cooperative effects. This requires doping that exceeds the solubility limit of III-V semiconductors. This problem was overcome by low-temperature nonequilibrium molecular beam epitaxial (MBE) growth. MBE is a physical deposition process (basically evaporation) that is carried out in ultra-high vacuum and at substrate temperature typically not exceeding 800 Celsius. Due to the unobstructed molecular flow of the species to be deposited and the chemical cleanliness of the substrate surface, highly controlled growth of very thin epitaxial layers is possible. However, segregation of impurities during MBE growth is an obstacle in obtaining high concentration of magnetic ions. In addition, after the sample is prepared and found to be ferromagnetic below T_C, it is usually necessary to show that ferromagnetism is not caused by the segregation of purely magnetic components, e. g. MnAs during the fabrication of (Ga, Mn)As, but that Mn has been randomly substituted in the host semiconductor instead. Usually, the quality of the samples is examined by observing the Reflection High Energy Electron Diffraction (RHEED) patterns which help to determine if there is any phase segregation [70].

As mentioned before, the possibility of using the spin as well as the charge of the electron for information processing will find tremendous application in technology and it is the basic idea of spin electronics or spintronics. In order for spintronics devices to work, polarized carriers have to be introduced into a semiconductor, for example using ferromagnetic contacts. However, these devices have not been fabricated yet. The main reason is that it is very difficult to inject net spin polarization directly from a metal into a semiconductor [71], due to the conductance mismatch between the two materials that will cause big suppression of spintronic effects. It is at this point where DMSs would become extremely useful because they would substitute the metallic contact and provide a FM contact that has a conductance similar to that of the semiconductor. Therefore, DMSs have many potential advantages over metals for the fabrication of spintronic devices. A theory of spin-polarized transport in inhomogeneous magnetic semiconductors has been developed in Ref. [72] similar to the standard theory of charge transport for p-n junctions. It is likely that these proposed applications for DMS will be realized only if ferromagnetism at room temperature can be achieved.

The transport properties of bulk materials and two dimensional structures are of great importance in materials' assessment particularly in developing and optimizing new device structures and highly affected by the phonon scattering, which is inherent to the solid state of matter. The electron mobility is influenced strongly by the interaction of electrons with phonons. The saturation velocity of carriers in a semiconductor provides the speed of a microelectronic device fabricated from this semiconductor [73]. Evidently, the practical switching time of such a microelectronic device will be limited by the saturation velocity and clearly therefore, the phonons play major role in the fundamental practical applications and limits of such microelectronic devices. The dynamics of carrier capture in the active quantum well region of a polar semiconductor quantum well LASER also introduces the importance of carrier-phonon interactions in modern semiconductor devices. It is observed that the loss of energy by an electron depends on the rates for both phonon absorption and phonon emission. Further, it is observed that the dimensional confinement of phonons in inter-sub-band semiconductor lasers changes the LASER gain and leads to enhanced population inversion in some asymmetric double barrier quantum well LASERs [74]. The dimensional confinement of phonons restricts the phase space of phonon wavevactor and hence, the carrier phonon interactions in nanostructures are modified by the phonon confinement. In the present chapter, we present the carrier-phonon scattering formulation for two dimensional nanostructures and its application to the dilute nitride alloys. The scattering rates have been calculated by using the deformation potential coupling mechanism which has been already described for the bulk structures in the previous chapter. This approach has been quite successfully used earlier in the case of bulk semiconductor and as well on its nanostructures [75, 76], but this is probably the first attempt in the case of dilute nitrides.

3.2 Phonon Scattering of Confined Carriers (2D)

In a bulk semiconductor, carriers are free to move in three dimensions, but in modern semiconductor devices, carriers are often confined in quantum wells where they can move only in two dimensions. Important examples are silicon MOSFETs and modulation doped III-V FETs where the carriers in the channel are confined near the surface in a potential well. The scattering rates for these two- dimensional carriers are different than for three dimensional carriers. The calculation of two- dimensional (2D) scattering rates proceeds much like it does for three-dimensional (3D) electrons, but the proper wave function for confined carriers is an essential aspect. The density of states for carriers in a quantum well is piecewise constant at

$$k_z = \frac{n\pi}{W} \tag{3.10}$$

where n=1,2,3............n_{max} and W is the width of quantum well. For an infinitely deep well, the envelop functions can be considered as

$$F_n(z) = \sqrt{2/W}\sin k_z z \tag{3.11}$$

In the case of quantum well, the electrons are confined in z-direction, but they are free to move in x-y plane. The total wave function for the electron is

$$\varphi(x,y,z) = F_n(z)\frac{e^{ik_p \cdot \rho}}{\sqrt{A}} \tag{3.12}$$

where, A is the cross-sectional area. Because the momentum in z-direction is quantized, the electron's energy is also quantized and expressed as

$$E = \varepsilon_n + \frac{\hbar^2 k_p^2}{2m^*} = \frac{n^2\hbar^2\pi^2}{2m^* W^2} + \frac{\hbar^2 k_p^2}{2m^*} \tag{3.13}$$

The matrix element due to perturbation required for carrier scattering rate given in previous chapter is given as

$$H_{p',p} = \int_{-\infty}^{+\infty} \varphi_{p'}^* U_s \varphi_p d^3r \tag{3.14}$$

The matrix element takes the form as

$$H_{pp'} = \int_{-\infty}^{+\infty} F_f^*(z)\frac{e^{-ip'_p \cdot \rho/\hbar}}{\sqrt{A}}\left(A_\beta K_\beta e^{\pm i\beta_p \cdot \rho} e^{\pm i\beta_z \cdot z}\right) F_i(z)\frac{e^{ip_p \cdot \rho/\hbar}}{\sqrt{A}} d\rho dz \tag{3.15}$$

where, subscript, i, refers to an initial subband, f, to the final subband and p is the parallel case, where use of initial and final wave functions

$$\varphi_{p'} = F_f(z)\frac{e^{ip'_p\cdot\rho/\hbar}}{\sqrt{A}}$$

and

$$\varphi_p = F_i(z)\frac{e^{ip_p\cdot\rho/\hbar}}{\sqrt{A}}$$

and perturbation potential $U_s = A_\beta K_\beta e^{\pm i\beta_p\cdot\rho} e^{\pm i\beta_z\cdot z}$ has been made to obtain the matrix element. The integral over the transverse plane gives a δ-function expressing momentum conservation in the plane so eq.(3.15) becomes

$$H_{pp'} = \int_{-\infty}^{+\infty} F_f^*(z)F_i(z)e^{\pm i\beta_z\cdot z}dz A_\beta K_\beta \frac{e^{-ip'_p\cdot\rho/\hbar}}{\sqrt{A}}\frac{e^{ip_p\cdot\rho/\hbar}}{\sqrt{A}}\left(e^{\pm i\beta_p\cdot\rho}\right)d\rho$$

$$= \int_{-\infty}^{+\infty} F_f^*(z)F_i(z)e^{\pm i\beta_z\cdot z}\left(e^{\pm i\beta_p\cdot\rho}\right)A_\beta K_\beta e^{\pm i\left(\beta_p\cdot\rho+\beta_z z\right)}dz$$

$$= \int_{-\infty}^{+\infty} F_f^*(z)F_i(z)e^{\pm i\beta_z\cdot z}A_\beta K_\beta \delta_{p'_p,\,p_p\pm\hbar\beta_p}dz \qquad (3.16)$$

$$S(p,p') = \frac{2\pi}{\hbar}\left|\int_{-\infty}^{+\infty} F_f^*(z)F_i(z)e^{\pm i\beta_z\cdot z}\right|^2 dz\left|A_\beta\right|^2\left|K_\beta\right|^2\delta_{p'_p,\,p_p\pm\hbar\beta_p}\,\delta\left(E'-E\mp\hbar\omega\right) \qquad (3.17)$$

Where, the integral $\int_{-\infty}^{+\infty} F_f^*(z)F_i(z)e^{\pm i\beta_z\cdot z}dz$ is called the form factor.

The transition rate is given as

$$\frac{1}{\tau} = \sum_{p'} S(p,p')$$

$$=\sum_{p'}\frac{2\pi}{\hbar}\left|\int_{-\infty}^{+\infty}F_f^{*}(z)F_i(z)e^{\pm i\beta_z\cdot z}\right|^{2}dz\left|A_\beta\right|^{2}\left|K_\beta\right|^{2}\delta_{p_p',p_p\pm\hbar\beta_p}\,\delta(E'-E\mp\hbar\omega)\qquad(3.18)$$

3.2.1 ADP Scattering Rate

The present section deals with the carrier scattering from the acoustic phonons which has been used to investigate the transport properties of dilute nitrides in the present work. Using eq. (2.30) and (2.29), where according to Bose-Einstein Distribution, the number of phonons to count the thermal energy is $N_\beta=\frac{K_BT_L}{\hbar\omega_\beta}$, therefore,

$$\left|A_\beta\right|^{2}=\frac{\hbar}{2\rho\Omega\omega_\beta}\left(\frac{K_BT_L}{\hbar\omega_\beta}+\tfrac{1}{2}\mp\tfrac{1}{2}\right)$$

$$\therefore\left|K_\beta\right|^{2}\left|A_\beta\right|^{2}=\beta^{2}D_A^{2}\frac{K_BT_L\hbar}{2\rho\Omega\omega_\beta^{2}}$$

$$=\frac{D_A^{2}K_BT_L}{2\left(\rho\omega_\beta^{2}/\beta^{2}\right)\Omega}=\frac{D_A^{2}K_BT_L}{2C_l\Omega}\qquad(3.19)$$

Where $C_l=\left(\rho\omega_\beta^{2}/\beta^{2}\right)$ is the elastic constant. $\boldsymbol{D_A}$ is the acoustic deformation potential (ADP) expressed as

$$D_A=K_BT_L\left(M/m*\right)^{1/2}\qquad(3.20)$$

Where, $m*\quad\frac{\hbar^{2}}{{}^{2}E/k^{2}}$ is electron effective mass and M is atomic mass (in g), which varies with lattice temperature. The scattering rate is expressed as

$$\frac{1}{\tau}=\frac{W}{2\pi}\left|A_{\beta}\right|^{2}\left|K_{\beta}\right|^{2}\int_{0}^{\infty}\left|F_{f}^{*}(z)F_{i}(z)e^{\pm i\beta_{z}\cdot z}\right|^{2}d\beta_{z}$$

$$=\frac{W}{2\pi}\frac{D_{A}^{2}K_{B}T_{L}}{2C_{l}\Omega}\int_{0}^{\infty}\left|F_{f}^{*}(z)F_{i}(z)e^{\pm i\beta_{z}\cdot z}\right|^{2}d\beta_{z}$$

$$=\frac{D_{A}^{2}K_{B}T_{L}}{4\pi C_{l}A}\int_{0}^{\infty}\left|F_{f}^{*}(z)F_{i}(z)e^{\pm i\beta_{z}\cdot z}\right|^{2}d\beta_{z}\qquad\frac{\Omega}{W}=A=Area$$

$$=\frac{D_{A}^{2}K_{B}T_{L}}{4\pi C_{l}A}\int_{-\infty}^{\infty}F_{f}^{*}(z)F_{i}(z)dz\int_{-\infty}^{+\infty}F_{f}^{*}(z')F_{i}^{*}(z)dz'\int_{-\infty}^{+\infty}e^{\pm i\beta_{z}\cdot(z-z')}d\beta_{z}$$

By using

$$\frac{1}{2\pi}\int_{0}^{\infty}e^{\pm i\beta_{z}(\beta-\beta')}d\beta_{z}=\delta(z-z'),\tag{3.21}$$

$$\frac{1}{\tau}=\frac{D_{A}^{2}K_{B}T_{L}}{2C_{l}A}\int_{-\infty}^{\infty}\left|F_{f}^{*}(z)\right|^{2}\left|F_{i}(z)\right|^{2}dz$$

$$=\frac{D_{A}^{2}K_{B}T_{L}}{2C_{l}A}\frac{1}{W_{fi}}\tag{3.22}$$

Where,

$\frac{1}{W_{fi}}=\int_{-\infty}^{\infty}\left|F_{f}^{*}(z)\right|^{2}\left|F_{i}(z)\right|^{2}dz$ is the effective extent of interaction in *z*- direction.

For intrasubband i.e. *i=f*,

$$\frac{1}{W_{fi}}=\frac{3}{2W}\tag{3.23}$$

and for intersubband i.e. $i\neq j$

$$\frac{1}{W_{fi}}=\frac{1}{W} \tag{3.24}$$

Therefore, the scattering rate for the two levels can be expressed as

$$\frac{1}{\tau_{fi}}=\sum_{p_p{}'}\frac{2\pi}{\hbar}\left(\frac{D_A^2K_BT_L}{2C_lA}\frac{1}{W_{fi}}\right)\delta_{p_p{}',p_p\pm\hbar\beta_p}\,\delta(E'-E\mp\hbar\omega)$$

$$=\left(\frac{\pi D_A^2K_BT_L}{\hbar C_lA}\frac{1}{W_{fi}}\right)\sum_{p_p{}'}\delta_{\mathbf{p_p}',\mathbf{p_p}\pm\hbar\boldsymbol{\beta}_\mathbf{p}}\,\delta(E'-E\mp\hbar\omega) \tag{3.25}$$

Here the summation in 3D and 2D results in just (1/2) of 3D DOS and (1/2) of 2D DOS respectively. Further to consider emission and absorption, we have to multiply by 2. Hence the final scattering rate of 2D carriers is,

$$\frac{1}{\tau_{fi}}=2\left(\frac{\pi D_A^2K_BT_L}{\hbar C_l}\frac{1}{W_{fi}}g_{2D}(E)\Big/2\right)$$

$$=\left(\frac{\pi D_A^2K_BT_L}{\hbar C_l}\frac{1}{W_{fi}}g_{2D}(E)\right) \tag{3.26}$$

$$=\left(\frac{\pi D_A^2K_BT_L}{\hbar C_l}\frac{1}{W}g_{2D}(E)\right)\quad \text{for intersubband} \tag{3.27}$$

and

$$=\left(\frac{\pi D_A^2K_BT_L}{\hbar C_l}\frac{3}{2W}g_{2D}(E)\right)\quad \text{for intrasubband} \tag{3.28}$$

The obtained carrier – acoustic phonon scattering can be used to obtain carrier acoustic phonon contribution to the resistivity using $\frac{m^*}{ne^2}$ where e is electronic charge, n is the number of charge carriers and τ is the carrier acoustic phonon relaxation time. The mobility of carrier in reference to the acoustic phonon is expressed as

$$\mu_{ac} = \frac{3.17\times 10^{-5}\, d u^{2}}{\left(m^{*}/m_{e} \right)^{5/2} D_{A}^{2} T^{3/2}} \tag{3.29}$$

where, d is the density of material , u is the average sound velocity, D_A is the acoustical deformation potential and T is absolute temperature. The sound velocity can be found out by the relation $u = \frac{k\theta_D}{\hbar}\left(\frac{V}{6\pi^2}\right)$ where θ_D Debye temperature is and V is average atomic volume, m_0 is rest mass.

3.2.2 ODP Scattering of Confined Carriers

We present here the carrier scattering from optical phonons by using deformation potential mechanism, however, in the present investigation, the scattering for acoustic phonons has only been considered at lower temperature. The first theoretical step was taken long ago by Fuchs and Kliewer [77] who described confined long wavelength and interface optical modes in a thin ionic slab. They described the ionic slab in terms of a dielectric continuum and the modes they obtained satisfied the usual electronic boundary conditions when there are no free charges, i.e. the continuity of tangential field and the normal component of the electronic displacement. They assumed that the longitudinally polarized (LO) and transversally polarized (TO) modes were dispersionless in the sense that does not depend upon the wavelength. This meant that there were no mechanical effects to worry about.

A microscopic model of an ionic slab by Jones and Fuchs [77] showed the simplicity of the dielectric continuum model (DC model) and observed the weak dispersion of LO and TO modes. This model was first applied to the problem of confined optical modes in semiconductor multilayer. In a direct gap polar-semiconductor an electron in conduction band interacts only with LO modes, via their long range electric fields and not at all with the TO modes. From the general analysis of Born and Huang [78], it can be deduced that the electric field, *E*, associated with an optical mode is related to the relative displacement of ions, *u*, as follows:

$$E = -\frac{S(\omega)\rho_i u}{\varepsilon_\infty} \qquad S(\omega) = \frac{\omega^2 - \omega_{TO}^2}{\omega_{LO}^2 - \omega_{TO}^2}$$

Where *S(ω)* is the field factor, Si is the ionic charge density and *εα* is the high frequency permittivity. Thus when $\omega = \omega_{LO}$, $\vec{E}$ is the LO field and when $\omega = \omega_{TO}$, the field $\vec{E}$ =0.

In the DC model, the allowed optical modes in a polar layer are determined only by electric boundary conditions and only the LO and interface modes need to be considered as these are the only waves that have electric fields. Because the permittivity vanishes for LO modes, the boundary conditions entail that the potential vanishes at an interface. The allowed modes in a quantum well formed by two barriers of the same material for symmetric case are

$$u_x = q_x A_{LO} e^{i(q_x x - \omega t)} \cos(q_z z) \quad u_z = i q_z A_{LO} e^{i(q_x x - \omega t)} \sin(q_z z) \qquad (3.30)$$

$q_z a = n\pi$; n=1, 3, 5...... $-\frac{a}{2} \le z \le \frac{a}{2}$

While for the antisymmetric form, this takes the form

$$u_x = iq_x A_{LO}\, e^{i(q_x x-\omega t)} \sin(q_z z) \qquad u_z = q_z A_{LO}\, e^{i(q_x x-\omega t)} \cos(q_z z) \tag{3.31}$$

$$q_z a = n\pi \ ;\ \text{n=2,4,6.....}\ ;\ -\frac{a}{2} \le z \le \frac{a}{2}$$

The DC model has been applied to structures other than a simple quantum well, the main examples of structures being quantum wells containing a monolayer [79, 80]. Quantum well with nearly metallic layers [61] and Quantum wires [82]. The optical modes predicted by the DC model are not those observed in Raman Scattering Experiments [83] nor are they those obtained in computationally intensive lattice dynamics calculations. It is hardly surprising that this is the case given the total neglect of mechanical boundary conditions in the DC model. Unfortunately it is not always clear regarding the boundary conditions. It is difficult to describe the nature of the optical mode stress in a continuum model. Modes in the barrier scatter electrons in the well via their associated interface mode fields. Summing the effects of all barrier hybrid modes turns out to be very close to the DC result for the barrier.

Carrier Scattering Rate:

Consider the interaction of an electron with longitudinal confined phonons in quantum wells. The confined phonons are 2D phonons. Their frequency depend on q and m, but because the dispersion of optical phonons is small in the long-wavelength limit, we can attribute the same frequency ω_{LO} to all confined modes.

We get the following projections of the vectors $\vec{w}_{\vec{q},m}(\rho, z)$ to the x-y plane and z-axis.

$$\left(\vec{w}_{\vec{q},m}\right)_{\rho} = \sqrt{2/SL}\,\frac{i\vec{q}H_m(z)}{\sqrt{q^2+\left(\pi m/L\right)^2}}\,e^{i\vec{q}\vec{\rho}} \qquad \left(\vec{w}_{\vec{q},m}\right) = \sqrt{2/SL}\,\frac{\frac{\pi m}{L}\,\frac{dH_m(z)}{dz}}{\sqrt{q^2+\left(\pi m/L\right)^2}}\,e^{i\vec{q}\vec{\rho}}$$

Here the function $H_m(z)$ corresponds to the symmetric and antisymmetric solutions in terms of eqs.

$$\phi_s = \phi_{0,s} e^{iq_x x} \cos q_z z \quad \phi_a = \phi_{0,a} e^{iq_x x} \sin q_z z$$

where, φ_0's are some amplitudes of the waves, and

$$H_m(z) = \cos(\pi m z/L) \;;\; \text{odd } m$$

$$= \sin(\pi m z/L) \;;\; \text{even } m$$

Having the explicit form of $\omega_{\vec{q},m}$, we can introduce the optical displacement associated with the particular solution $\vec{u}^{(O)} = Q_{\vec{q},m} w_{\vec{q},m}$ as well as the polarization $P = \gamma \vec{u}^{(O)}$. Then we calculate the electrostatic potential

$$-e\phi_{\vec{q},m}(\vec{\rho},z) = -4\pi e\gamma \sqrt{2/SL} \frac{Q_{\vec{q},m} H_m(z)}{\sqrt{q^2 + (\pi m/L)^2}} e^{i\vec{q}\vec{\rho}} \tag{3.32}$$

From this procedure, we get the coupling of electrons and confined LO phonons:

$$\Gamma(\vec{r}|\vec{q},m,LO) = -4\pi e\gamma \sqrt{\hbar V_0 / SLM\omega_{LO}} \frac{H_m(z)}{\sqrt{q^2 + (\pi m/L)^2}} e^{i\vec{q}\vec{\rho}} \tag{3.33}$$

$$\Gamma(n_0,k_0,\vec{k}|\vec{q},m,LO) = -4\pi e\gamma \sqrt{\hbar V_0 / SLM\omega_{LO}} \sqrt{\frac{G_{n0,n,m}}{q^2 + (\pi m/L)^2}} \delta_{\vec{k},\vec{k}+\vec{q}} \tag{3.34}$$

Here,$G_{n0,n,m}$ is the square of the overlap integral that can be calculated analytically:

$$G_{n0,n,m} = \left[\frac{2}{L} \int_{-L/2}^{L/2} dz \cos\left(\frac{\pi n_0 z}{L}\right) \cos\left(\frac{\pi n z}{L}\right) H_m(z) \right]^2$$

$$=\frac{32(n0nm)^2\left[1-(-1)^{n_0+n+m}\right]}{\pi^2\left[m^2-(n_0+n)^2\right]^2\left[m^2-(n_0-n)^2\right]^2} \tag{3.35}$$

Finally the scattering rate is expressed as,

$$\frac{1}{\tau_s(k_0,n_0)}=\frac{2e^2\omega_{LO}}{L}\left(\frac{1}{k_\infty}-\frac{1}{k_0}\right)\left(N_{LO}+\frac{1}{2}\pm\frac{1}{2}\right)$$

$$\times\sum_{n,m} G_{n_0,n,m}\int d^2q\frac{\delta\left(E_n(k_0+q)-E_{n0}(\overline{k_0})\mp\hbar\omega_{LO}\right)}{q^2+\left(\frac{\pi m}{L}\right)^2} \tag{3.36}$$

We can draw qualitative conclusions from these formulas. It can be seen from the equation (3.36) that the coupling factor, in contrast to the case of acoustic phonons, decreases with the decease of well width. The interaction of carriers with the LO phonons is the primary phonon mechanism responsible for scattering at temperatures above few tens of degrees Kelvin.

3.3 Results and Discussion

In the present section, we describe the results obtained on the *relaxation rates* due to acoustic phonons via deformation potential for the *diluted nitride semiconductors* and the diluted magnetic semiconductors (DMS) alloys. This section will also deal with the important conclusion carried out on the basis of results obtained from the present study. In the present calculation of the relaxation rate the inter-subband scattering is induced by the ADP scattering is considered. In this case the acoustic phonons carry little energy, so an electric field accelerates carriers to the energies exceeding the bottom of the next subband before scattering to a higher subband. The doping of nitrogen in GaAs is considered at the interstitial position which is shown in the Fig. 3.2.

3.3.1 Dilute Nitride Semiconductors

The acoustic phonon scattering rates calculated by using Eq. (3.27) for the two-dimensional $GaAs_{1-x}N_x$ alloys of 6 nm quantum well width at room temperature have been presented in Fig. 3.3. The input parameters for the calculation of scattering rates are presented in Table 3.1. The temperature and nitrogen concentration dependent acoustic deformation potential (ADP) D_A is used in the present calculation for $GaAs_{1-x}N_x$ system is obtained from the value of ADP of GaAs and GaN due to the nonavailability of the same for $GaAs_{1-x}N_x$. It is seen from table 3.1 that the ADP values show minor variation with the change in nitrogen concentration and temperature. Similar variation is also observed for the effective mass of carriers and elastic constant. The Figure 3.3 reveals that the scattering rate decreases with the increase in nitrogen concentration. This is due to the reduction of bandgap with the increase of nitrogen concentration [11, 12, 17]. The unexpectedly strong effect of nitrogen on the band gap is due to the fact that the replacement of arsenic atoms with the much smaller and more electronegative nitrogen atoms. This results in to a large, local perturbation of the crystal lattice potential. However, only a minor effect on the lattice constant of the resulting alloy is observed from the small content of nitrogen.

Nitrogen Concentration (x %)	**Effective mass ratio (m*)**	**Elastic constant C_l (GPa)**	**D_A (eV)**
0.000	0.065	119.00	52.25
0.001	0.0651	120.66	52.20
0.002	0.0652	122.34	52.15
0.006	0.0656	129.09	51.90
0.008	0.0658	132.52	51.80
0.010	0.0660	135.66	51.70

Table 3.1 Acoustic Deformation Potential D_A and Elastic Constant C_l for different nitrogen concentration.

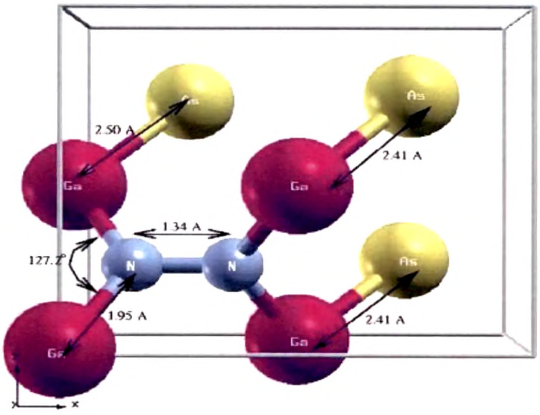

Fig, 3.2 *The equilibrium configuration of GaAsN.*

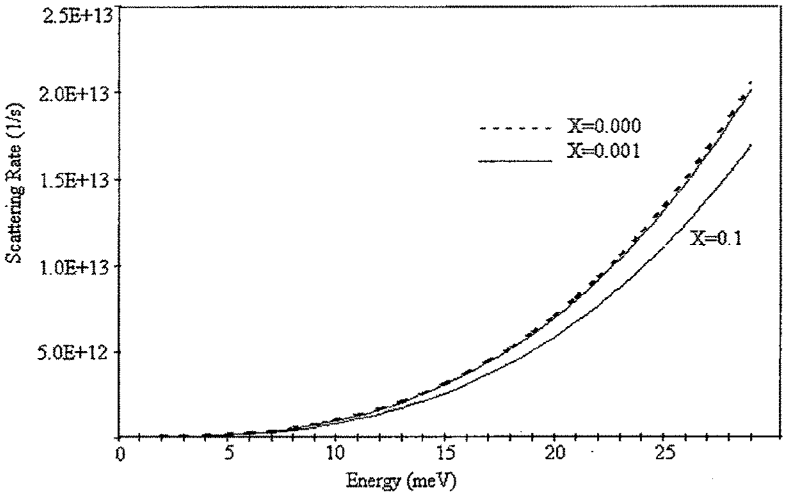

Fig 3.3 Variation of scattering rate with thermal energy for different nitrogen concentration in $GaAs_{1-x}N_x$.

The Fig.3.1 depicts that there is a significant change in the scattering rate even with 0.1% of nitrogen doping in GaAs. Here, we consider the maximum extent of diluted concentration of nitrogen below 10% as beyond this segregation may take place for GaAsN alloys. The N is isolelectronic with arsenic (As) and it behaves more like impurity atom than conventional alloying element. Due to a resonant interaction of a nitrogen state with the bottom of the conduction band, the bandgap is reduced in this dilute nitride alloys. Similar observation is made for the Bi alloy and it is believed to be due to a resonant interaction with the top of the valence band. However, the trend of scattering rates remains similar for all '*x*'. We have also investigated the effect of quantum well width on the acoustic phonon scattering rates for dilute nitride alloys $GaAs_{0.9}N_{0.1}$. But, we present the graph only for $GaAs_{0.9}N_{0.1}$ in figure 3.4. The Figure 3.4 reveals that the scattering rate decreases as the width of quantum well increases. This is due to the fact that the effective extent of interaction in *z*- direction decreases, which is more prominent in intrasubband.

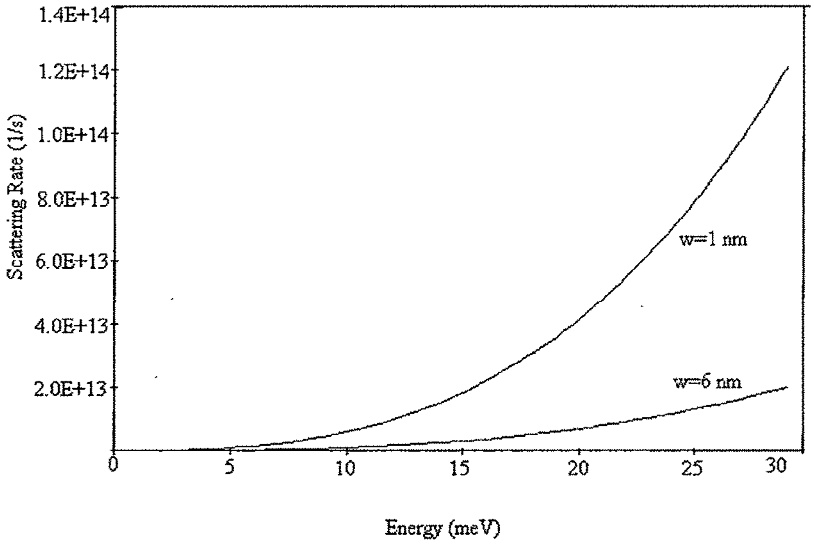

Fig.3.4 Variation of scattering rate with thermal energy for different quantum well widths of $GaAs_{1-x}N_x$.

3.3.2 Diluted Magnetic Semiconductors

The electron acoustic phonon scattering rates calculated by using Eq. (3.27) for the two-dimensional $Ga_{(1-x)}Mn_xN$ alloy (for $0.0<x< 0.1$) have been presented in Figure 3.5. In the present calculation of scattering rate for 2D DMS alloys, no effect of spin is included, which is separately dealt in chapter 5. The scattering rate for all considered concentration of Mn increases with the energy which shows similar behaviour and almost same value in the case of lower energies but varies exponentially for higher energies. The inset shows the high energy variation of electron-acoustical phonon scattering rate. This increase of scattering rate at higher energy is due to the fact that the deformation potential increases due to the increase of phonon density of states resulting from confinement of phonons and restriction of phase space. It is important to see and understand the effect of Mn concentration on scattering rate, we have also calculated the scattering rate for different Mn concentration. The Figure 3.6 presents the variation of scattering rate with the Mn concentration which reveals that the scattering rate decreases with increase in Mn concentration. This is due to the simultaneous increase of effective mass and total atomic mass. However, the effect of atomic mass is more significant than the effective mass on ADP (kindly see table 3.2). The Fig, 3.7 shows the behaviour of acoustic deformation potential (ADP) with energy and Mn concentration. It is seen form the figure that the ADP increases with energy but decreases with the concentration. To understand the role of Mn on acoustic phonon contribution to the resistivity of the reference material GaN,

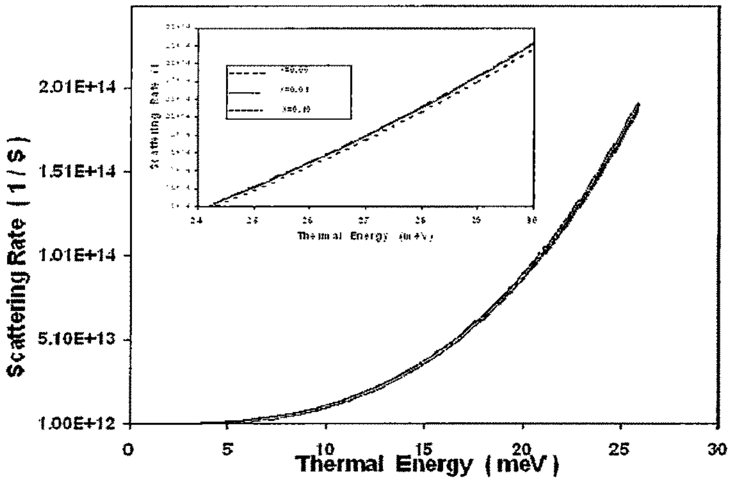

Fig.3.5 Variation of acoustic phonon scattering rates for two-dimensional $Ga_{1-x}Mn_xN$ with manganese concentration and thermal energy.

we have calculated the resistivity of two dimensional alloy and presented them in Fig. 3.8. The inset shows the variation of scattering rate with Mn concentration. The resistivity increases but its increase is faster for higher concentration of Mn similar to scattering rate. The calculation of total resistivity by considering all different scattering mechanism is in progress.

Concentration x (≤0.1)	**Effective mass ($\times 10^{-28}$ gm)**	**D_A (in eV)**
0.000	2.0020	21.61
0.001	2.0843	21.16
0.002	2.1860	20.66
0.003	2.2766	20.25
0.004	2.3720	19.84
0.005	2.5180	19.25
0.006	2.6278	18.84
0.007	2.7420	18.44
0.008	2.8998	17.96
0.009	2.9610	17.74
0.010	3.1086	17.31
0.100	13.010	08.39

Table3.2 Effective mass and deformation potential for 2-dimensional $Ga_{(1-x)}Mn_xN$.

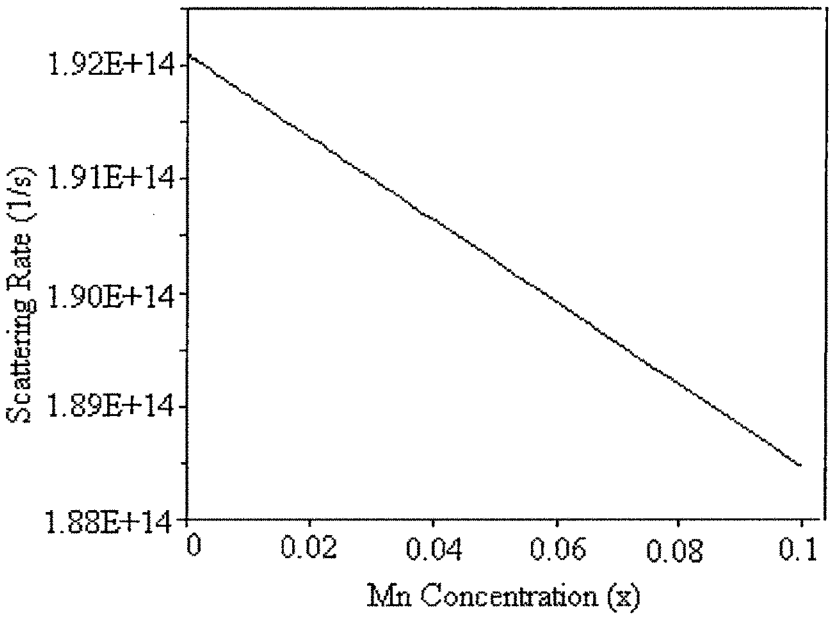

***Fig.3.6** The variation of scattering rate with manganese concentration.*

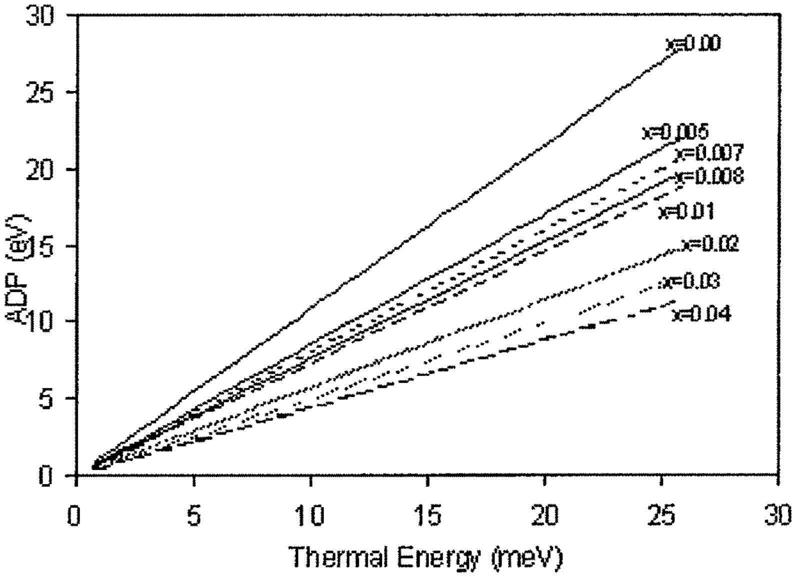

Fig.3.7 Variation of acoustical deformation potential (ADP) with manganese concentration and thermal energy.

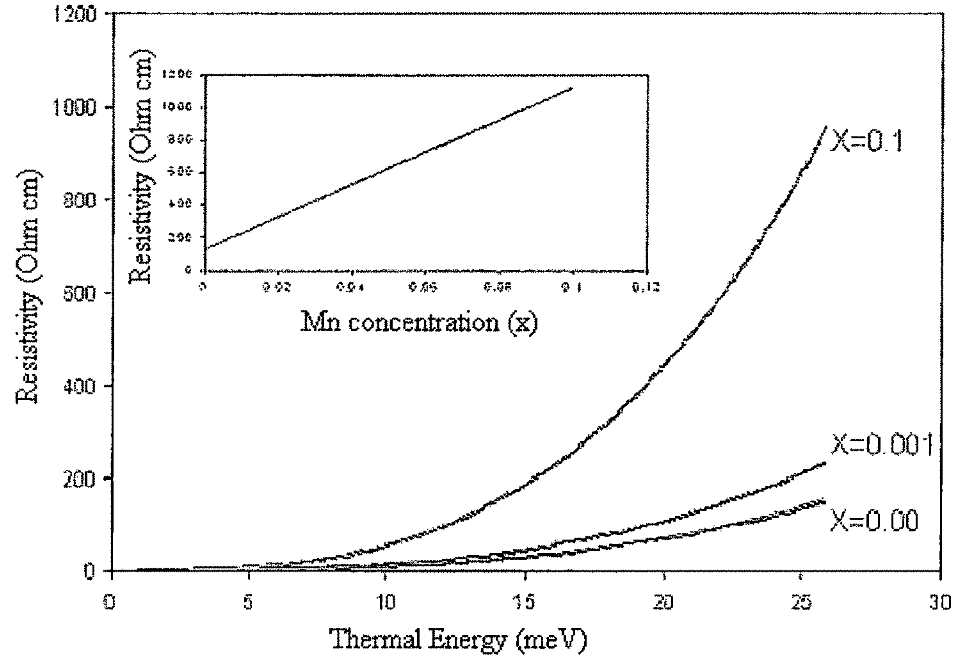

Fig.3.8 Resistivity variation with thermal energy and manganese concentration.

3.4 Summary

We have calculated the acoustic phonon scattering rate for the two dimensional $GaAs'_{1-x}N_x$ and $Ga_{1-x}Mn_xN$ nanostructure for different well widths and concentrations. The width of the well as well as the concentration of nitrogen and manganese in host influences the carrier acoustic phonon scattering rates. The reduction of scattering due to the increases in concentration is attributed to the reduction of band gap of two dimensional diluted nitrogen alloys. This reduction of band gap influences the acoustic deformation potential which in principle is main quantity directly influencing the scattering rate and transport properties.

References

1. S Nakamura, G Fasol, The Blue Laser Diode (Springer, Berlin, 1997); S N Mohammad, H Morkoc, Prog. Quantum Electron. **20**, 361(1996) I Akasaki, H Amano, *Jpn. J. Appl. Phys.* **36,** 5393 (1997) and references therein.
2. M C Larson, M Kondow, T Kitatani, Y Yazawa and M Okai *Electron. Lett.* **33,** 959 (1997).
3. M C Larson, M Kondow, T Kitatani, K Tamura, Y Yazawa and M Okai *IEEE Photon. Technol. Lett.* **9,** 1549 (1997).
4. M C Larson, M Kondow, T Kitatani, K Nakahara, K Tamura, H Inoue and K Uomi *IEEE Photon. Technol. Lett.* **10,** 188(1998).
5. C Ellmers, F Hohnsdorf, J Koch, C Agert, S Leu, D Karaiskaj, M Hofmann, W Stolz and W W Ruhle *Appl. Phys. Lett.* **74,** 2271 (1999).
6. A Wagner, C Ellmers, F,Hohnsdorf, J Koch, C Agert, S Leu, M Hofmann, W Stolz and WW Ruhle *Appl. Phys. Lett.* **76,** 271 (2000).
7. C W Coldren, M C Larson, S G Spruytte and J S Harris, *Electron. Lett.* **36,** 951 (2000).
8. J B Heroux, X Yang and W Wang, *Appl. Phys. Lett.* **75,** 2716 (1999).
9. S R Kurtz, A A Allerman, E D Jones, J M Gee, J J Banas and B E Hammons , *Appl. Phys. Lett.* **74,** 729 (1999).
10. H P Xin, C W Tu and M Geva, *Appl. Phys. Lett.* **75,** 1416 (1999).
11. K Uesugi, N Marooka and I Suemune, *Appl. Phys. Lett.* **74,** 1254 (1999).
12. M Kondow, K Uomi, A Niwa, T Kitatani, S Watahiki and Y Yazawa, *Japan. J. Appl. Phys.* **35,** 1273 (1996).

13. C Skierbiszewski et al. *Appl. Phys. Lett.* **76,** 2409 (2000).

14. J F Geisz, D J Friedman, J M Oslon, S R Kurtz, M B Keyes, *J. Cryst. Growth,* **195,** 401(1998).

15. W Shan et al., *Phys. Rev Lett.* **82,** 1221(1999).

16. J D Perkins et al., *Phys. Rev. Lett.* **82,** 3312(1999).

17. H P Xin, C W Tu, *Appl.Phys. Lett.,***72,** 2442(1998).

18. X Liu, S G Bishop, J N Baillargeon, K Y Cheng, *Appl. Phys. Lett.*, **63,** 208 (1993).

19. M Weyers, M Sato, H Ando, *Jap. J. Appl.Phys.*, **31,** 4413 (1993).

20. A Rubio, M L Cohen, *Phys. Rev.***B51,** 4343 (1995).

21. S Sakai, Y Ueta, Y Terauchi, *Jap. J. Appl. Phys.*, **32,** 4413(1993).

22. W Shan et al., *Phys. Rev. Lett.* **82,** 1221 (1999).

23. W Wulukiewicz et al., *The Elecrrochemical Soc.Pennington,* NJ, 199 (1999).

24. J Neugebauer and C G Van de Walle, *Phys. Rev.* ***B*****51,** 10568 (1995).

25. C T Foxon et al *J. Cryst. Growth* **150,** 892(1995).

26. W G Bi and C W Tu, *Appl.* Phys. Lett. 70, 1608 (1997).

27. R J Potter, N Balkan, M J Adams, P R Chalker, T B Joyce and T J Bullough *SPIE* (parts 1 and 2) **3944** 900–9 ISBN: 0-8194-3561 (2000).

28. M Sopanen, H P Xin and C W Tu, *Appl. Phys. Lett.* **76,** 994(2000).

29. D G Thomas, J J Hopfield and C J Frosch, *Phys. Rev. Lett.,* **15,** 857 (1965).

30. D. G. Thomas and J. J. Hopfield, *Phys. Rev Lett.,* **150,** 680 (1966).

31. D J Wolford, J A Bradley, K Fry and J Thompson, *Proceedings of the 17th International Conference on the Physics of Semiconductors*, edited by J.D. Chadi and W.A. Harrison, Springer-Verlag, New York, 627(1984).

32. X Liu, M E Pistol, L Samuelson, S Schwetlick and W Seifert, *Appl. Phys. Lett*, **56**, 1451 (1990).
33. X Liu, M E Pistol and L Samuelson, *Phys. Rev. B*, **42**, 7504 (1990).
34. M Weyers, M Sato, H Ando, *Jpn. J. Appl. Phys. Pt. 2.*, **31**, L853 (1992).
35. M Kondow, K Uomi, K Hosomi, T Mozume, *Jpn. J. Appl. Phys.*, **33**, L1056 (1994)
36. S H Wei, A Zunger, *Phys. Rev. Lett.*, **76**, 664 (1996).
37. P N Hai, W M Chen, I A Buyanova, H P Xin and C W Tu, *Appl. Phys. Lett*, **77**, 1843 (2000).
38. Z Pan, L H Li, Y W Lin, B Q Sun, D S Jiang, W K Ge, *Appl. Phys. Lett*, **78**, 2217 (2001).
39. M H Gass, A J Papworth, T B Joyce, T J Bullough, and P R Chalker, *Appl. Phys. Lett*, **84**, 1453(2004).
40. C Skierbiszewski, I Gorczyca, S P £epkowski, J Lusakowski, J Borysiuk and J Toivonen, *Semicond. Sci.Technol.*, **19**, 1189 (2004).
41. F Masia, A Polimeni, G Baldassarri Höger von Högersthal, M Bissiri, M Capizzi, P J Klar and W Stolz, *Appl. Phys. Lett*, **82**, 4474 (2003).
42. F Masia, G Pettinari, A Polimeni, M Felici, A Miriametro, M Capizzi, A Lindsay, S B Healy, E P O'Reilly, A Cristofoli, G Bais, M Piccin, S Rubini, F Martelli, A Franciosi, P J Klar, K Volz, W Stolz, *Phys. Rev. B***73**, 073201 (2006).
43. W Shan, W Walukiewicz, J W Ager , E E Haller, J F Geisz, D J Friedman, J M Olson, S R Kurtz, *Phys. Rev. Lett.*, **82**, 1221 (1999).

44. W Shan, W Walukiewicz, J W Ager III, E E Haller, J F Geisz, D J Friedman, J M Olson, S R Kurtz, J. *Appl. Phys.*, **86**, 2349 (1999).

45. K Uesugi, I Suemune, T Hasegawa, T Akutagawa, T Nakamura, *Appl. Phys. Lett*, **76**, 1285 (2000).

46. H P Hjalmarson, P Vogl, D J Wolford and J D Dow, *Phys. Rev. Lett.*, **44**, 810 (1980)

47. A Rubio and M L Cohen, *Phys. Rev. B***51**, 4343 (1995)

48. J Neugebauer and C G Van de Walle, *Phys. Rev. B***51**, 10568 (1995)

49. S Wei and A Zunger, *Phys. Rev. Lett.*, **76**, 664 (1996)

50. A Lindsay and E P O'Reilly, *Solid State Commun.*, **112**, 443 (1999)

51. J Wu, W Walukiewicz and E E Haller, *Phys. Rev. B***65**, 233210 (2002)

52. E P O'Reilly, A Lindsay, S Tomic and M Kamal-Saad, *Semicond. Sci. Technol.*, **17**, 870 (2002).

53. P Vogl, *Adv. Electron. Electron Phys.*, **62**, 101 (1984).

54. L Bellaiche, S H Wei and A Zunger, *Phys. Rev. B***54**, 17568 (1996).

55. T Mattila, S H Wei and A Zunger, *Phys. Rev. B***60**, R11245 (1999).

56. P R C Kent and A Zunger, *Phys. Rev. Lett.*, **86**, 2613 (2001).

57. P R C Kent and A Zunger, *Phys. Rev. B***64**, 115208 (2001).

58. P R C Kent, L Bellaiche, A Zunger, *Semicond. Sci. Technol.*, **17**, 851 (2002).

59. P N Keating, *Phys. Rev.* **B145**, 637 (1966).

60. R M Martin, *Phys. Rev.* **B1**, 4005 (1970).

61. A Lindsay and E P O'Reilly, *Physica E***21**, 901 (2004).

62. E P O'Reilly, A Lindsay, S Fahy, *J.Phys.:Condens Matter* **16**, S3257 (2004).

63. A Lindsay, E P O'Reilly, *Phys. Rev. Lett.*, **93**, 196402 (2004).

64. H Ohno, *Science*, **281**, 951 (1998).

65. F E Arkun et al., *Appl. Phys. Lett.,* **85,** 3809 (2004).

66. L Kronik, M Jain, J R Chelikowski, *Phys. Rev.* ***B*66,** 041203 (2002).

67. R Y Korotkov, B W Weseels, *Appl. Phys. Lett.* **80,** 1458 (2002).

68. H Ohno, A Shen, F Matsukura, A Oiwa, A Endo, S Katsumoto, and Y Iye, *Appl. Phys. Lett.*, **69**,363 (1996).

69. H Ohno, H Munekata, T Penney, S von Molnar, and L L Chang, *Phys. Rev. Lett.* **68,** 2664(1992).

70. H Hori, S Sonoda, T Sasaki, Y Yamamoto, S Shimizu, K Suga, and K Kindo. *Physica* **B324,** 142 (2002).

71. M Johnson, *Semicond. Sci. Technol.,* **17,** 298 (2002).

72. I Zutic, J Fabian, and S. Das Sarma, Phys. Rev. Lett., **88**,066603 (2002).

73. P Chang, A Baca & N Li, Appl. Phys. Lett **76,** 2262 (2000).

74. Y Ohno, *Nature*, **402,** 787(1999).

75. S Dutta & B Das, *Appl Phys.Lett.* **56,** 665 (1990).

76. M Combescot & J Bok, *Phys Rev* ***B*35**, 1181 (1987).

77. R Lassnig, *Phys. Rev.* ***B*30,** 7132 (1984).

78. M Born and K Huang, Dynamical theory of crystal lattices (Clarendon, Oxford).

79. J Pozela, V Juciene, K Pozela, Semicond. sci. Technol. 1076 (1995).

80. B K Ridley, M Babiker, N Zakhleniuk et al., *Proc. ICPS-23*, Berlin (1996).

81. N Constantinou, *Phys.Rev* ***B*48,** 11931 (1993).

82. C R Bennett et al, *J. Phys. Condens. Matter* 7, 9819 (1995).

83. A K Sood, J Menendez, M Cardona, *Phys. Rev. Lett.* **54,** 211 (1985).